1 # Multifunctional Tin Dioxide Materials: Advances in Preparation

2 # Strategies, Microstructure, and Performance

3 **Zhiwen Chen,**[*abc] **Minghong Wu,**[*ab] **Chan-Hung Shek,**[*c] **C. M. Lawrence Wu,**[c] **and Joseph K. L.**

4 **Lai**[c]

5 [a] *Shanghai Applied Radiation Institute, Shanghai University, Shanghai 200444, People's Republic of*

6 *China*

7 [b] *School of Environmental and Chemical Engineering, Shanghai University, Shanghai 200444,*

8 *People's Republic of China*

9 [c] *Department of Physics and Materials Science, City University of Hong Kong, Tat Chee Avenue,*

10 *Kowloon Tong, Hong Kong*

11

12

13

14

15

[a] *Shanghai Applied Radiation Institute, Shanghai University, Shanghai 200444, People's Republic of China. E-mail: zwchen@shu.edu.cn. Tel.: +86 21 66137503; Fax: +86 21 66137787.*

[b] *School of Environmental and Chemical Engineering, Shanghai University, Shanghai 200444, People's Republic of China. E-mail: mhwu@staff.shu.edu.cn.*

[c] *Department of Physics and Materials Science, City University of Hong Kong, Tat Chee Avenue, Kowloon Tong, Hong Kong. E-mail: apchshek@cityu.edu.hk*

16   **Abstract**

17   Tin oxide materials are a class of unique semiconductor materials with widespread technological

18   applications because of their valuable semiconducting, gas sensing, electrical and optical properties in

19   the fields of macro/mesoscopic materials and micro/nanodevices. In this review, we describe the efforts

20   toward understanding the synthetic strategies and formation mechanisms of the micro/nanostructures of

21   various tin dioxide thin films prepared by pulsed laser ablation, highlighting contributions from our

22   laboratory. First, we present the preparation and formation processes of tetragonal-phase tin dioxide

23   thin films with interesting fractal clusters. In addition, the quantum-dot formation and dynamic scaling

24   behavior in tetragonal-phase tin dioxide thin films induced by pulsed delivery will be discussed

25   experimentally and theoretically. Finally, we emphasize the fabrication, properties and formation

26   mechanism of orthorhombic-phase tin dioxide thin films by using pulsed laser deposition. This

27   research may provide a novel approach to modulate their competent performance and promote rational

28   design of micro/nanodevices. Once mastered, tin dioxide thin films with a variety of fascinating

29   micro/nanostructures will offer vast and unforeseen opportunities in semiconductor industry as well as

30   in other fields of science and technology.

31

32   **Keywords:** Tin Oxides; Thin Films; Preparation Strategies; Microstructure; Performance

33

34

35

36

37

1. Introduction

38

39 The key scientific issues of semiconductor micro/nanodevices and optoelectronics components in

40 application and development have been driven scientists to explore in depth the design, preparation,

41 micro/nanostructure and performance of semiconductor materials.[1-5] Semiconductor oxides are

42 fundamental to the development of smart and functional materials, devices, and systems. Tin oxide

43 materials have two unique structural features: mixed cation valences and an adjustable oxygen

44 deficiency, which are the bases for creating and tuning many novel material properties, from chemical

45 to physical. Tin oxide micro/nanostructures have garnered considerable attention in recent years for

46 their potential to facilitate both the fundamental research and practical applications through their

47 advantageous chemical and physical properties.[6-8] An integrated device for semiconductor industry is

48 highly desirable for versatile advanced applications.[9-11] The prospect of using pulsed laser deposition

49 processes to fabricate semiconductor oxide thin films continues to drive research towards improving

50 the performance of the semiconducting materials utilized in these devices. Since the properties of

51 materials strongly depend on its micro/nanostructures, which all result from the fabrication processes,

52 the influence of micro/nanostructural evolution on material properties is especially remarkable for

53 materials science and engineering.[12,13] However, challenges remain to further improve the material

54 fabrication processes for various advanced applications. This optimization requires a clear

55 understanding of the relationship between micro/nanostructures and thin film morphologies.[14,15]

56 Tin oxide micro/nanostructures provide a versatile, multifaceted platform for a broad range of

57 advanced applications.[16] Recent studies have validated their use in many fields of science and

58 technology that integrate the areas of chemistry, physics, materials science and nanotechnology. For

59 example, they can function as semiconductors for a number of applications in microelectronic devices,

60 optoelectronic components, and solar-thermal converter, they can serve as gas-sensors for the detection

61 and forecasting of a variety of combustible gases, environmental pollution gases, industrial emissions

62   and hazardous gases, they can used as electrodes for melting optical glass and electrolytic aluminum

63   industry, they can act as catalysts for the active phase of many heterogeneous catalysis in hydrocarbon

64   oxidation, they can also serve as varistor for the arrester used in power systems, and so on.

65   Tin dioxide (SnO_2) thin films are essential components of several modern technologies. For instance,

66   SnO_2 thin films represent an unsurpassed material in the design of metal oxide gas-sensors,[17,18] and the

67   microelectronic revolution would have not been the same without the excellent properties of SnO_2 thin

68   films. However, SnO_2 thin films with fascinating micro/nanostructures are often used in many sundry

69   devices and systems. For example, it is used as the lithium-ion battery anode materials, gas-sensing

70   materials, negative temperature coefficient thermistor materials, doped SnO_2 varistor materials,

71   resistance-type humidity-sensing materials, catalyst materials, optical and electrical materials, etc. the

72   possibility to growth micro/nanostructures is therefore essential to improve the performance of SnO_2

73   thin films.[19] Several synthetic strategies have been developed to grow the SnO_2 thin films and study

74   their chemistry.[20,21] In fact, significant advances have been done in the understanding of the

75   micro/nanostructural evolution of SnO_2 thin films.[22,23] However, it is only in the past few years that it

76   became evident that besides SnO_2 thin films that closely resemble the corresponding bulk materials,

77   also new systems exist, sometimes with unexpected properties either related to the morphologies of

78   SnO_2 thin films or to their micro/nanostructural flexibility. Presumably, the most exciting

79   developments are related to the possibility to modify in a desired manner the chemical properties of

80   molecules or deposited SnO_2 thin films with fascinating micro/nanostructures.[24,25] Most of above

81   applications are based upon the novel micro/nanostructures known as derived from different synthetic

82   strategies and processing.[26-28] Pulsed laser deposition (PLD) technique is considered to be one of the

83   effective methods for the preparation of SnO_2 thin films with fascinating micro/nanostructures.

84   PLD is a useful growth tool in which photonic energy is coupled to the bulk starting material via

85   electronic processes.[29,30] Laser ablation for thin film growth has many advantages: (i) energy source

86   (laser) is outside the vacuum chamber, in contrast to vacuum-installed devices, which provides a much

87   greater degree of flexibility in materials used and geometrical arrangements; (ii) almost any condensed

88   matter material can be ablated; (iii) pulsed nature means that thin film growth rates may be finely

89   controlled; (iv) amount of evaporated source material is localized only to that area defined by the laser

90   focus; (v) under optimal conditions, the ratios of the elemental components of the bulk and thin films

91   are the same, even for chemically complex systems; (vi) kinetic energies of the ablated species lie

92   mainly in a range that promotes surface mobility while avoiding bulk displacements; and (vii) ability to

93   produce species with electronic states far from chemical equilibrium opens up the potential to produce

94   novel or metastable materials that would be unattainable under thermal conditions. Above growth

95   processes may be supplemented by an inert or reactive gas or ion source, which may affect the ablation

96   plume species in the gas phase or surface reaction. The diversity of thin films grown by using PLD is

97   enormous and perhaps recommends its flexibility more persuasively than anything else.

98   During the past ten years or so, we and our collaborators have actively devoted in the investigations

99   of the micro/nanostructures of tin oxide thin films that related to the synthesis methods, technological

100   improvements, characterizations, properties and applications. This review only covers some of the most

101   recent studies, with a focus on their synthetic strategies and formation mechanisms. We start with a

102   detailed investigation of the preparation and formation processes of tetragonal-phase SnO_2 thin films

103   with interesting fractal clusters. We then describe experimentally and theoretically the quantum dot

104   formation and dynamic scaling behavior in tetragonal-phase SnO_2 thin films induced by pulsed

105   delivery. Finally, we elaborate on the fabrication, properties and formation mechanism of

106   orthorhombic-phase SnO_2 thin films. Fig. 1 shows schematic illustrating the morphological changes

107   involved in the tetragonal SnO_2 fractal thin films, tetragonal SnO_2 quantum dots and orthorhombic

108   SnO_2 thin films prepared by laser ablation.

109
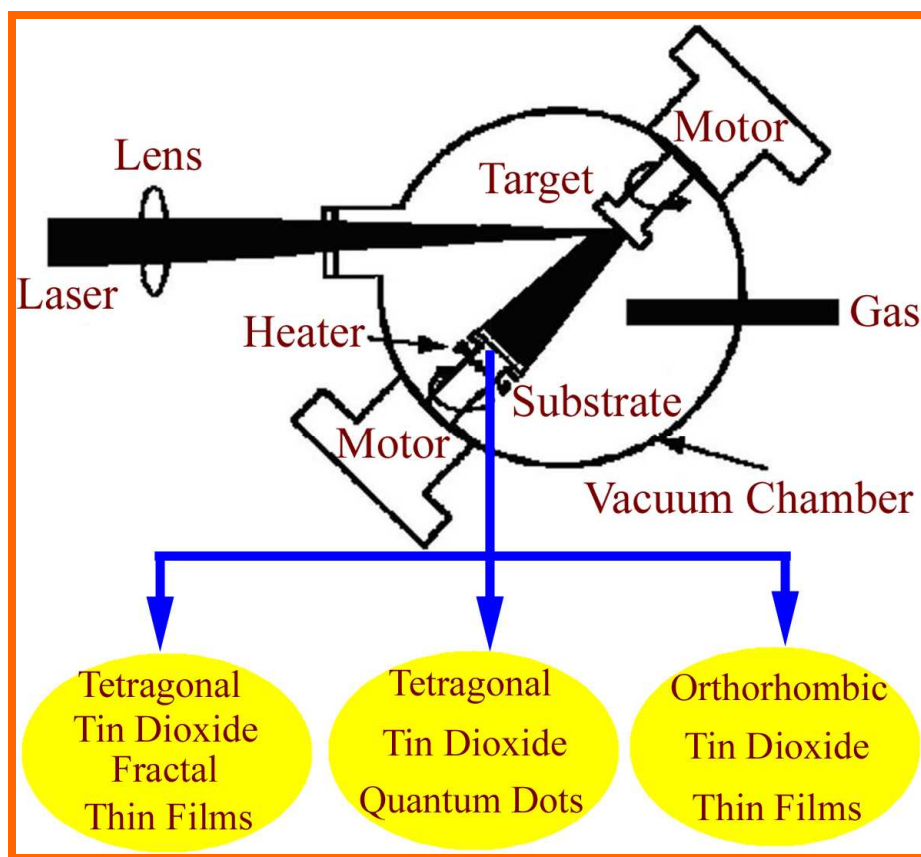
Fig. 1 Schematic illustrating the morphological changes involved in the tetragonal SnO_2 fractal thin

films, tetragonal SnO_2 quantum dots and orthorhombic SnO_2 thin films prepared by laser ablation.

112

2. Tin dioxide fractal thin films

With the advent of advanced thin film technology more cost-effective, reproducible devices can be

constructed with a reduction in device size and a concomitant increase in the response speed by using

SnO_2 thin films. Since gas sensing is based on adsorption mechanism on the SnO_2 grain surface, a

small grain size is desirable in order to achieve a high specific area for high sensitivity.[31,32] Structural

properties, such as grain size, grain geometry as well as specific surface area, can significantly affect

the gas sensing properties of SnO_2 thin films. In order to control these structural characteristics, the

micro/nanostructural evolution of SnO_2 thin films should be understood. Micro/nanostructural

121   variations should inevitably change their chemical and physical properties. Thus, the study of the

122   micro/nanostructures of SnO_2 grains can help us to reveal some peculiar micro/nanoscale features and

123   to explain the corresponding experimental results.

124   Fractal theory is a potentially powerful technique to characterize micro/nanostructures. We and our

125   collaborators have successfully applied this technique to the fractal assessment of SnO_2 thin films.[33,34]

126   Besides showing some examples of geometric structures of SnO_2 thin films, here we will discuss the

127   applicability and relevance of fractal theory to studying the micro/nanostructure and formation

128   mechanism of SnO_2 thin films. Fig. 2 shows the scanning electron microscopy (SEM) images of SnO_2

129   thin films prepared on Si (100) substrate at temperatures of (A) 300, (B) 350, (C) 400, and (D) 450°C,

130   respectively. SEM observation indicated that all thin films produced under different substrate

131   temperatures exhibited self-similar fractal patterns. It can be seen that the fractal patterns are open and

132   loose structure with increasing substrate temperature. The average size and fractal dimension (D) of the

133   fractal clusters for four thin films were estimated by measurement on the fractal regions and using

134   conventional box-counting method,[35-37] respectively, which were decided to be about 0.307 μm (Fig.

135   3A) with $D = 1.896$, 0.906 μm (Fig. 3B) with $D = 1.884$, 1.202 μm (Fig. 3C) with $D = 1.865$, and 1.608

136   μm (Fig. 3D) with $D = 1.818$. It was found that the average size of the fractal clusters increased and the

137   fractal dimension decreased with increasing substrate temperature. The smaller fractal dimension

138   means that the SnO_2 thin films are composed of the open and loose fractal structure with finer branches.

139   This fractal structure may lead to improvement in the design of gas sensors for the monitoring of

140   environmental pollutants.
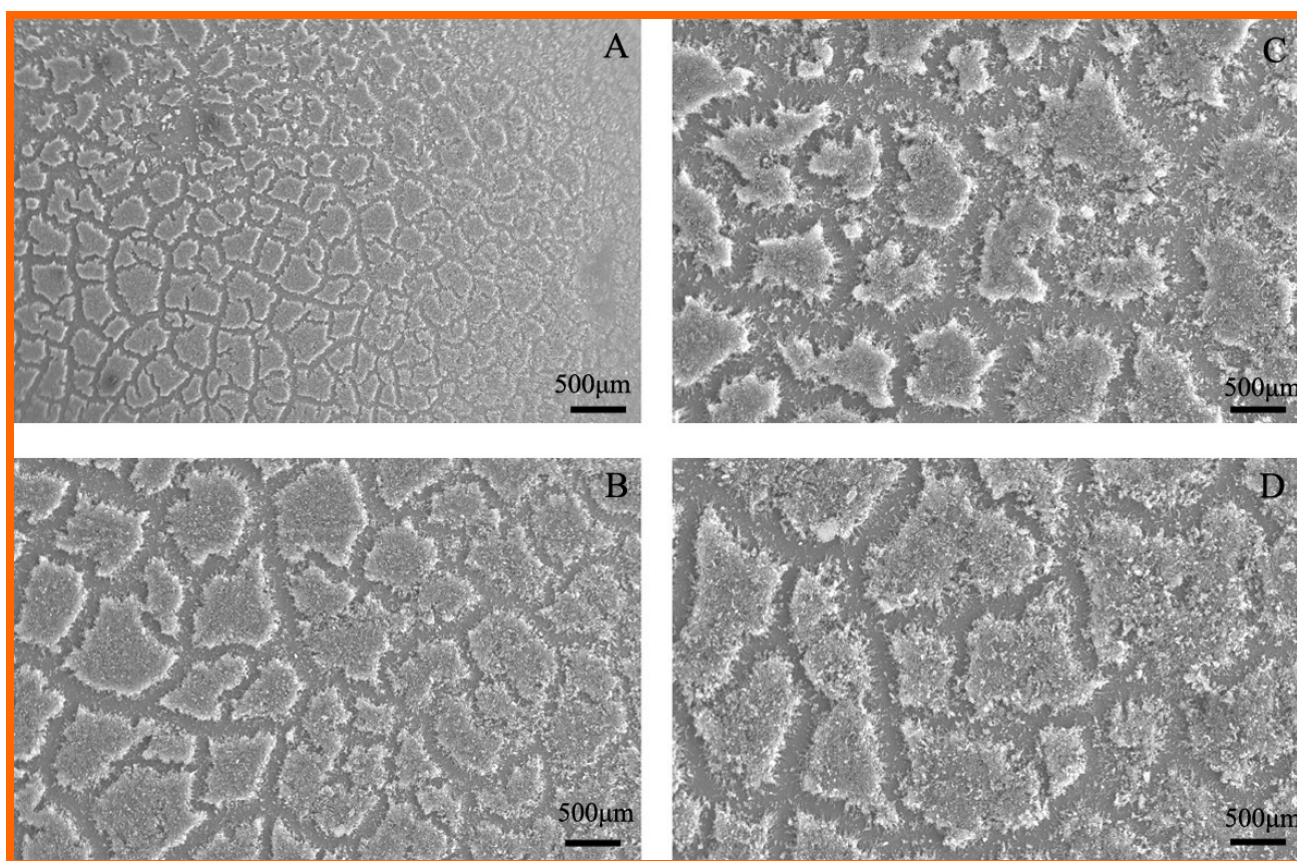
Fig. 2 SEM images of SnO$_2$ thin films prepared on Si (100) substrate at temperatures of (A) 300; (B) 350; (C) 400; and (D) 450°C.[33]

On the basis of experimental observation, the formation process of SnO$_2$ nanocrystals and fractal clusters could be reasonably described by a novel model proposed by us.[33] It was separated into eight steps, which illustrated in detail in Fig. 3: (i) operation of the KrF excimer laser at a repetition rate of 10 Hz at an incident angle of 45° to the polished sintered cassiterite SnO$_2$ target rotating at a rate of 15 rpm to avoid drilling; (ii) production of the high-temperature and high-pressure SnO$_2$ plasma at the solid-liquid interface quickly after the interaction between the pulsed laser and SnO$_2$ target; (iii) subsequent expansion of the high-temperature and high-pressure SnO$_2$ plasma leading to cooling of the SnO$_2$ plumes.[38,39] In this case, the interval between two successive pulses is much longer than the life

153   of the plasma. Therefore, the next laser pulse had no interaction with the former plasma; (iv) deposition

154   of the SnO_2 plume on Si (100) substrate after the disappearance of the plasma, inducing the initial

155   nucleation of SnO_2 nanocrystals; (v) grain rotation culminating in a low-energy configuration. This

156   process is directly related to the reduction of surface energy, aimed at minimizing the area of high-

157   energy interfaces;[40] (vi) possible formation of a coherent boundary between grains due to grain rotation,

158   with the consequence of removing the common grain boundary and culminating in a single larger SnO_2

159   nanocrystal. This is the coalescence process; (vii) growth of SnO_2 nanocrystals along preferred

160   crystallographic directions which could be predicted by an analysis of the surface energy in several

161   crystallographic orientations; (viii) formation of the fractal structure as SnO_2 crystallizes and nucleates

162   at high energy interfaces such as grains boundaries. According to the fractal theory, the heat released

163   by crystallization leads to a local temperature rise in surrounding area and this temperature field can

164   propagate quickly and stimulate new nuclei appearing randomly in nearby regions. The stimulated

165   nuclei of the next generation can also cause a local temperature rise and repeat the above process many

166   times until SnO_2 fractal patterns are formed.[41,42] Based on the above proposed formation mechanism,

167   we characterized the formation processes of SnO_2 fractal clusters as shown in Fig. 3A~I. We believe

168   that the laser ablation technique is an appropriate method to synthesize a series of fractal clusters with

169   controlled composition, morphology and nanocrystal size, which are of important in the study of the

170   sensitivity of SnO_2 thin films.
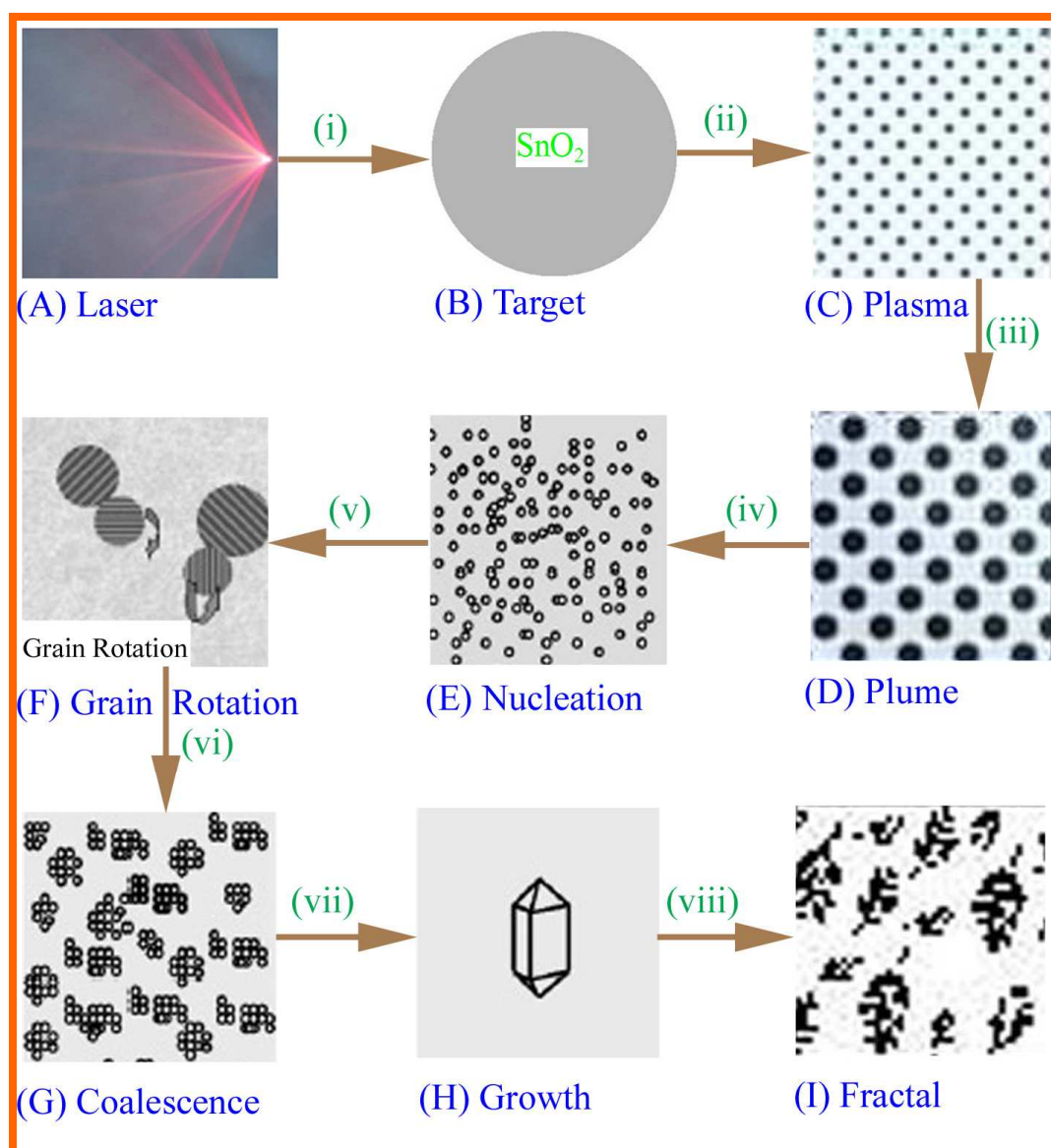
Fig. 3 The formation processes of SnO_2 nanocrystals and fractal clusters: (A) laser; (B) target; (C) plasma; (D) plume; (E) nucleation; (F) grain rotation; (G) coalescence; (H) growth; and (I) fractal.[33]

3. Tin dioxide quantum dots

In a variety of nonequilibrium growth processes, such as gelation, aggregation, coagulation, and condensation, the formation of size-distributed clusters is a very commonly encountered phenomenon. Therefore, understanding the related dynamics is a problem of considerable interest. Many studies on

179   this subject have revealed the scale invariance of the cluster size distribution. Among the various

180   processes involving cluster/droplet growth and coalescence, the process of vapor deposition has been

181   most widely investigated, a few examples being the role of condensate patterns in heat transfer, breath-

182   figure formation, and thin film growth. We have successfully demonstrated experimentally and

183   theoretically the quantum dot formation and dynamic scaling behavior of SnO_2 nanocrystals induced by

184   pulsed delivery.[43] Fig. 4 shows a high-resolution transmission electron microscopy (HRTEM) image of

185   the as-deposited SnO_2 thin films prepared by PLD method. It can be seen that the clear-cut crystalline

186   features inside the SnO_2 thin films. On closer inspection, recurrent values of separation distance

187   between lattice layers were found (in particular, 0.33 nm, evidenced in the bottom left-hand corner

188   inset of Fig. 4), corresponding to lattice parameters of the rutile structure of SnO_2 cassiterite phase

189   (arising from <110> reflection). HRTEM investigation can give useful information about local

190   composition at dislocation cores. As can clearly be seen in Fig. 4, the grain cluster is composed of

191   several primary nanocrystallites without grain boundaries. This is strong evidence that the coalescence

192   occurs when two or more neighbor grains assume the same orientation, resulting in a single

193   nanocrystal. When nanocrystalline materials grow by oriented attachment at crystallographically

194   specific surfaces, there is a small misorientation at the interface. Spiral growth at two or more closely

195   spaced screw dislocations provides a mechanism for generating complex structures.[40] When the grains

196   assume the same orientation, that is, a coherent grain-grain boundary, the grain boundary must migrate

197   toward the smaller particle, resulting in a single larger nanocrystal.[42] We suggest that these

198   nanocrystals are composed of isolated SnO_2 nanocrystals about from 4 to10 nm in size that are

199   besieged by amorphous phase. This structure should result in the quantum dots of SnO_2 nanocrystals.

200   The local HRTEM image revealed that individual SnO_2 nanocrystal embedded isolatedly in an

201   amorphous matrix, which confirmed that the existence of the quantum dots is due to the reduction of

202   the grain size by pulsed delivery. It is reasonable to speculate that the crystalline quantum dots may

203   lead to further enhancement of the energy gap due to low-dimensional confinement. This quantum dot

204   distribution is in agreement with previous simulations based on the kinetic Monte-Carlo model.[43]
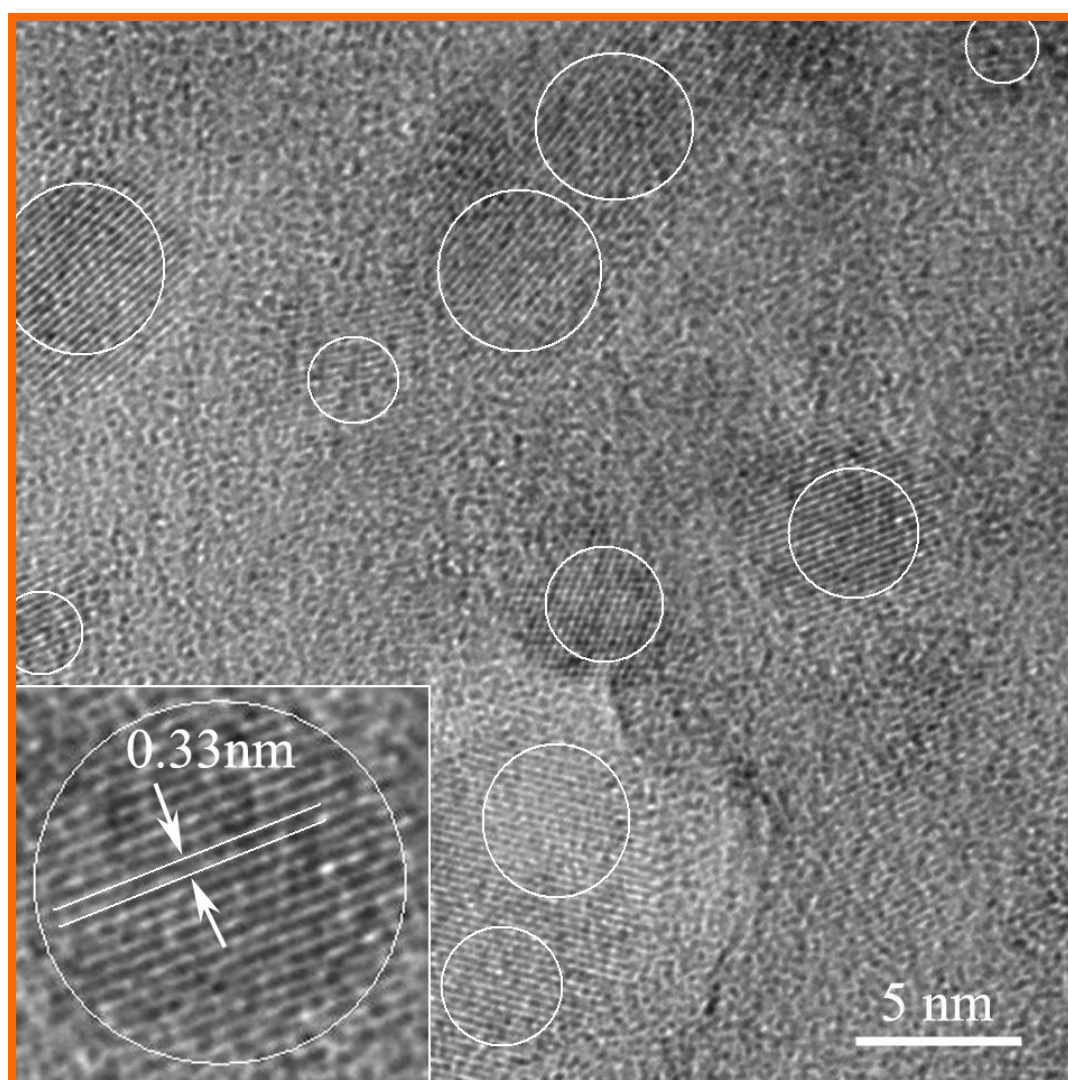
205

206   **Fig. 4** HRTEM image of the as-prepared SnO_2 thin films shows the structural features of the crystalline

207   nanophase; the bottom left-hand corner inset shows a magnification of the image of a single SnO_2 dot

208   5.5 nm in diameter in (110) plane with the measured lattice parameters.[43]

209

210   Fig. 5 shows the kinetic Monte-Carlo simulations of pulsed-laser deposition (Fig. 5a) and molecular-

211   beam epitaxy (MBE) (Fig. 5b) in the submonolayer regime. This model is controlled by three

212 parameters: the pulse intensity I, the diffusion constant D, and the average flux density of incoming

213 particles F. In particular, the control parameter of PLD is the pulse intensity I, which is the number of

214 particles deposited in one pulse per unit area, and the diffusion-to-deposition ratio D/F. The average

215 deposition rate is given by $F = I/\Delta t$, where Δt is the time interval between two pulses. The intensity is

216 measured in monolayers (ML), and D/F is dimensionless, as the lattice constant is set to unity.

217 Performing Monte-Carlo simulations, we investigated the nucleation density for various pulse

218 intensities using a system size of 400×400 square lattice and the island distance has been measured at

219 0.2 ML coverage, when the island density reaches its maximum but coalescence does not yet set in. For

220 small intensities, we recover the well-known power law for the island distance in MBE:[44]

221
$$l_D \propto (D/F)^\gamma, \qquad (1)$$

222 where the exponent γ depending on the dimension of the surface, the island dimension, and the critical

223 nucleus i^*, that is, the smallest stable island contains i^*+1 atoms. For a two-dimensional surface,

224 compact islands and a critical nucleus of $i^* = 1$, one obtains $\gamma = 1/6$. Here, one should note that the

225 islands are not compact but fractal patterns as shown in Fig. 5b. This is due to the fact that edge

226 diffusion is not considered in the simulations. The exponent γ can be determined from simulations such

227 that one monitors the number of nucleation events in a layer ($\propto l_D^{-2}$) as a function of D/F. However, for

228 PLD with large intensities, the island distance obeys a different power law:

229
$$l_D \propto I^{-\nu}, \qquad (2)$$

230 where $\nu = \gamma/(1-2\gamma) = 1/(2+d_f)$, and more generally $\gamma = 1/(4+d_f)$, if they have the fractal

231 dimension d_f. In this regime the island distance is independent of the parameter D/F, since the adatoms

232 do not make use of their diffusion probability, as they find an island and attach to it in a much shorter

233 time as the time they are allowed to diffuse between two depositions. Therefore, above two regimes

234   described by the formulae (1) and (2) are separated by a crossover at a certain intensity, where the

235   number of deposited atoms is of the same order of magnitude as the adatom density. As the average

236   adatom density n in MBE scales as $n \propto (D/F)^{-1+2\gamma}$, the critical intensity has to show the same scaling

237   behavior: $I_c \propto (D/F)^{-1+2\gamma}$. The qualitative difference between PLD and MBE for $I > I_c$ is shown in Fig.

238   5. As can be seen, there are many nucleations at an early stage, although the effective flux of incoming

239   particles is the same in both cases. The scaling behavior, namely, the fractal dimension, is measured by

240   using the box-counting method. The fractal dimension values for the PLD and MBE were decided to be

241   1.28±0.03 and 1.62±0.03, respectively. The scaling exponent was found to be significantly different as

242   compared to the exponent for the same system under continuous vapor deposition such as MBE. The

243   simulations revealed that this attractive difference could be pursued to the large fraction of multiple

244   droplet coalescence under pulsed vapor delivery.

245
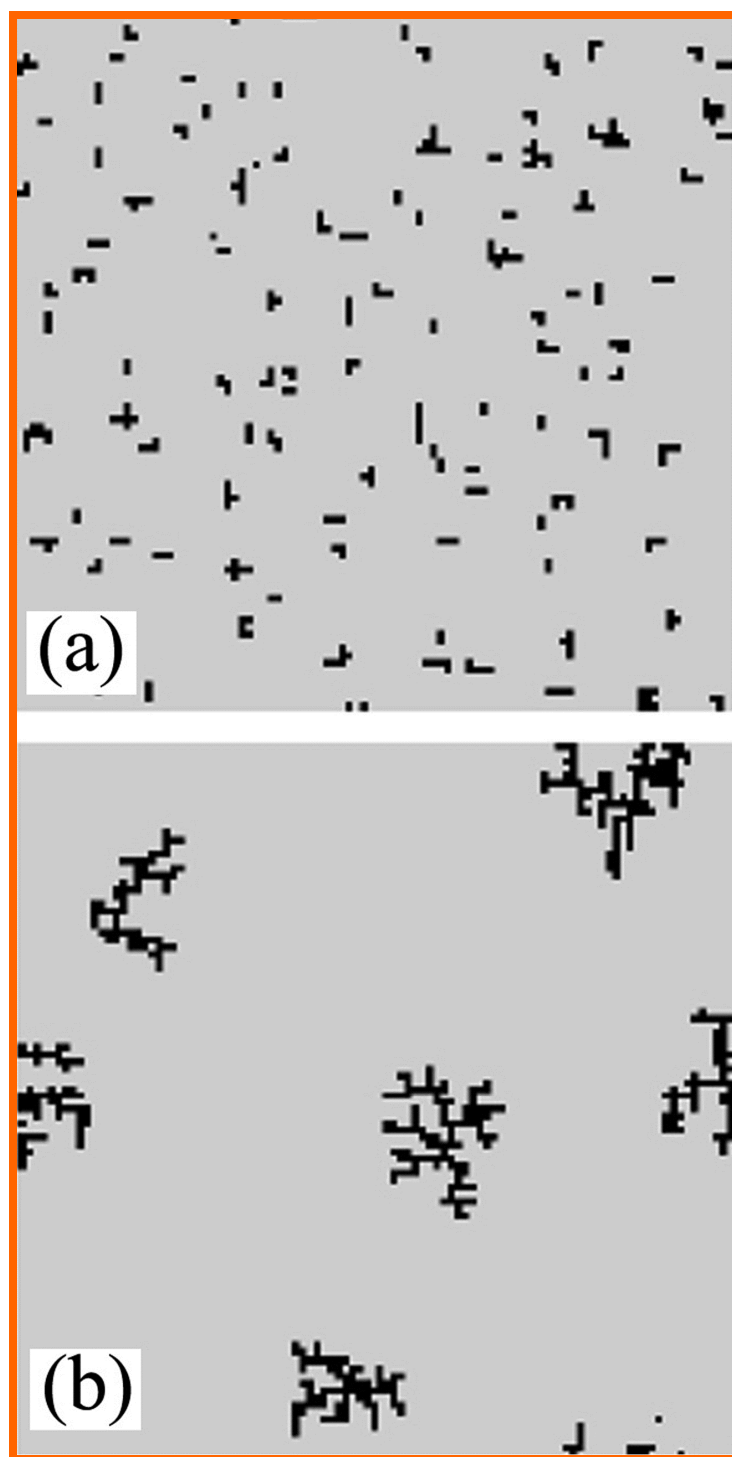
Fig. 5 The kinetic Monte-Carlo simulations of pulsed-laser deposition and molecular-beam epitaxy in the submonolayer regime. (a) A simulated PLD-grown surface with $D/F = 2 \times 10^8$ and $I = 0.01$ ML; (b) A simulated MBE-grown surface with $D/F = 2 \times 10^8$. The figure shows typical configurations after deposition of 0.05 ML.[43]

4. Orthorhombic tin dioxide thin films

It has been known that the naturally occurring form of SnO_2 is cassiterite. Under normal conditions, SnO_2 exists in the most important form of a crystalline phase known as cassiterite. The cassiterite has a rutile tetragonal crystal structure and its optical, electrical and gas-sensing properties have been extensively studied.[22,23] Sangaletti and co-workers have reported SnO_2 multilayer thin film grown by the rheotaxial growth and thermal oxidation method on Al_2O_3 substrates.[45] Their results indicated that, in addition to the SnO_2 cassiterite phase, a contribution from another SnO_2 phase was present, which can be related to cassiterite by introducing micro-twinning effects. This SnO_2 multilayer thin film showed a higher sensitivity towards CO with respect to the conventional single layer SnO_2 sensors. Another form of SnO_2 with an orthorhombic structure is known to be stable only at high pressures and temperatures. The formation of orthorhombic-phase SnO_2 is intimately tied to a number of important synthesis parameters such as high pressures and temperatures.[46-48] Müller found an unknown epitaxial interface phase of SnO_2 on α-quartz $(10\bar{1}0)$, which indicated that different octahedra stacking in the case of SnO_2 may give rise to different orthorhombic possibilities.[49] Several authors have claimed the "discovery" of this "high-pressure" phase under low-pressure conditions.[50-53] Arbiol and co-workers have reported the synthesis of pure monocrystalline orthorhombic SnO_2 nanowires and pure monocrystalline orthorhombic SnO_2 nanowires decorated with cassiterite SnO_2 nanoclusters.[54] In fact, when previous experiments are examined in detail, it is often difficult to rule out the possibility of the presence of high compressive stress. Here, we highlight our experimental results of orthorhombic SnO_2 thin film under low pressure and temperature by using pulsed laser deposition technique.[55]

The X-ray diffraction (XRD) patterns of the as-prepared thin films (Fig. 6a-i) indicated that the major reflections can be indexed to the orthorhombic-phase SnO_2 (labeled O) referred to the International Center for Diffraction Data PDF file as shown in Fig. 6a-iii. Upon exposing the as-prepared thin films to ambient air for six months, the intensity and position of the XRD patterns remain

274 unchanged (Fig. 6a-ii). This result revealed that the as-prepared thin films are stable and have an

275 orthorhombic SnO_2 structure. However, it seems that some reflections can also be assigned to the

276 tetragonal-phase SnO (labeled T). Above results proved that the as-prepared thin films may be a

277 mixture matrix of the orthorhombic-phase SnO_2 and tetragonal-phase SnO. Further investigation of the

278 phase purity of the as-prepared thin films is necessary. Fig. 6b shows the X-ray photoelectron spectra

279 (XPS) taken from the tin and oxygen regions. The peaks at 495.0 and 486.5 eV are attributed to the

280 $Sn3d_{3/2}$ and $Sn3d_{5/2}$, respectively, which are close to the data for Sn($3d$) in SnO_2. The gap between the

281 $Sn3d_{3/2}$ and $Sn3d_{5/2}$ levels is 8.5 eV which is approximately the same as that in the standard spectrum

282 of Sn. The peak at 530.5 eV can be assigned to the O1s (the inset in Fig. 6b). Owing to the proximity of

283 the XRD patterns and XPS peaks of SnO_2 and SnO, the valence states of tin species of the as-prepared

284 thin films could not be satisfactorily determined from the XRD and XPS results. Fig. 7a represents the

285 room-temperature experimental Mössbauer spectrum for the as-prepared thin films as well as its fitting

286 curve. Clearly, only one absorbing peak appears here, with an isomer shift and a quadruple splitting

287 being 0 and ~0.6 mm/s, respectively. From data analysis, it is concluded that the tin shows a Sn^{4+}

288 valence state. The energy-dispersive X-ray spectroscopy (EDXS) analysis revealed that the as-prepared

289 thin films are composed of 33.4 at.% Sn and 66.6 at.% O (Fig. 7b), that is, Sn:O = 1:1.994, which is in

290 good agreement with Sn:O = 1:2 of SnO_2 bulk. The above results indicated that the chemical

291 composition of the as-prepared thin films is consistent with the SnO_2 form.

17
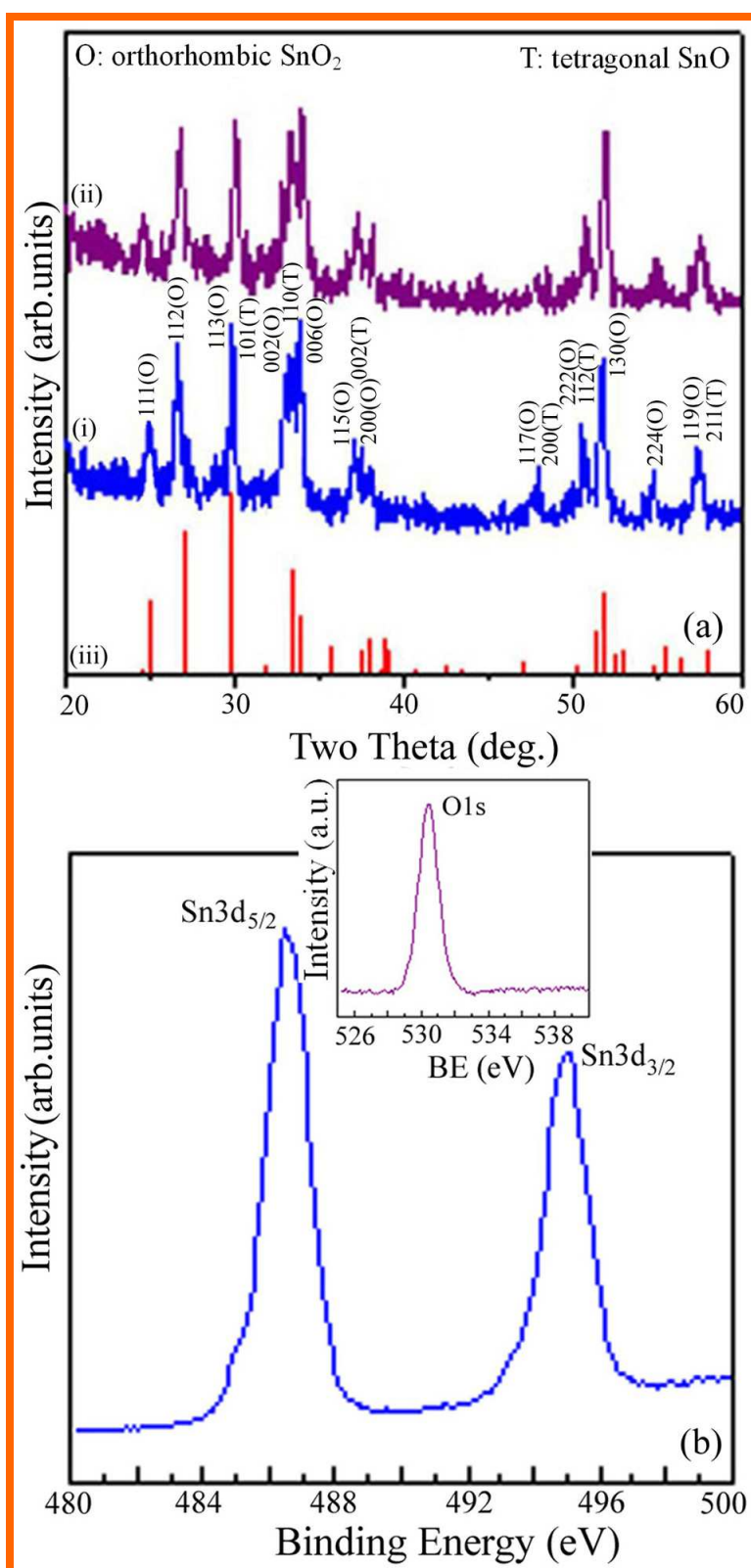
292

293

294 **Fig. 6** (a) XRD patterns of (i) the as-prepared SnO_2 thin film (orthorhombic SnO_2 labeled O and tetragonal SnO labeled T); (ii) exposing the as-prepared SnO_2 thin film to ambient air for six months;

295   (iii) the standard SnO_2 bulk. (b) XPS of the as-prepared SnO_2 thin film, which was taken from the tin

296   and oxygen regions.[55]

297
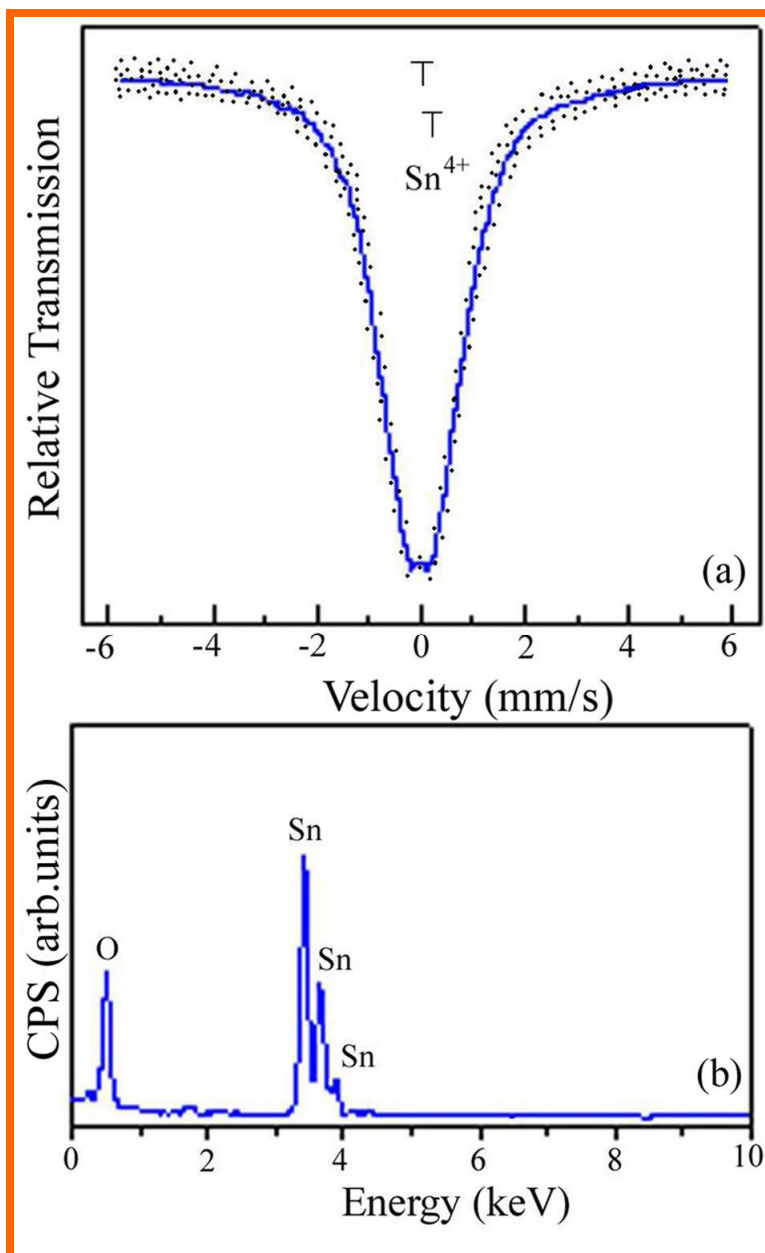
298   **Fig. 7** (a) Room-temperature experimental Mössbauer spectrum for the as-prepared SnO_2 thin film and

299   its fitting curve. (b) EDXS of the as-prepared SnO_2 thin film.[55]

300

301   Since the applications of SnO_2 are related to surface electronic properties, we further examined the

302   electronic structure of the orthorhombic SnO_2 thin films using soft X-ray absorption near-edge

303   structure (XANES) spectroscopy. A comparison of the Sn $M_{4,5}$-edge XANES spectrum of the

304   orthorhombic SnO_2 thin films to those of the tetragonal SnO_2 and SnO reference samples is given in

305   Fig. 8a. The Sn $M_{4,5}$-edge spectra reflected electron transitions from Sn$3d$ core level (spin-orbit split

306   into $3d_{3/2}$ and $3d_{5/2}$ levels, giving rise to M_4 and M_5 edges, respectively) to unoccupied electronic states

307   above the Fermi level. If the core hole and electron correlation effects are ignored, such spectra

308   essentially depicted Sn-related p- and f-projected states in the conduction band. Nevertheless, it is

309   important to note that the surface electronic structure of the orthorhombic SnO_2 is more similar to that

310   of the tetragonal SnO_2 rather than the tetragonal SnO. The data in Fig. 8a show that undercoordinated

311   surface atoms in the orthorhombic SnO_2 thin films introduce additional Sn-related electronic states,

312   which are close to the conduction band minimum (~499 eV in Fig. 8a). This finding is surprising. It is

313   consistent with the Mössbauer and EDXS analysis which revealed no evidence of the tetragonal-phase

314   SnO, and rules out the existence of the tetragonal SnO in XRD. The evaluation of above all

315   experimental data indicated that the as-prepared thin films are composed of a pure orthorhombic-phase

316   SnO_2. Fig. 8b shows that the optical transmittance is measured in the wavelength range from 200-800

317   nm for the orthorhombic SnO_2 thin films and tetragonal SnO_2 reference sample at room temperature.

318   We found that the transparency of the orthorhombic SnO_2 is superior to that of the tetragonal SnO_2. Fig.

319   8c shows the absorption coefficient versus the photon energy for the orthorhombic SnO_2 and tetragonal

320   SnO_2 reference sample. A linear extrapolation towards zero absorption E_g corresponds to direct allowed

321   transitions. We obtained E_g = 4.02 eV for the orthorhombic SnO_2 and E_g = 3.73 eV for the tetragonal

322   SnO_2 reference sample in energy. By comparing E_g for the orthorhombic SnO_2 thin films with that of

323   the tetragonal SnO_2 reference sample, it is evident that the band-gap widening occurs and hence the

324   orthorhombic SnO_2 thin films becomes transparent.
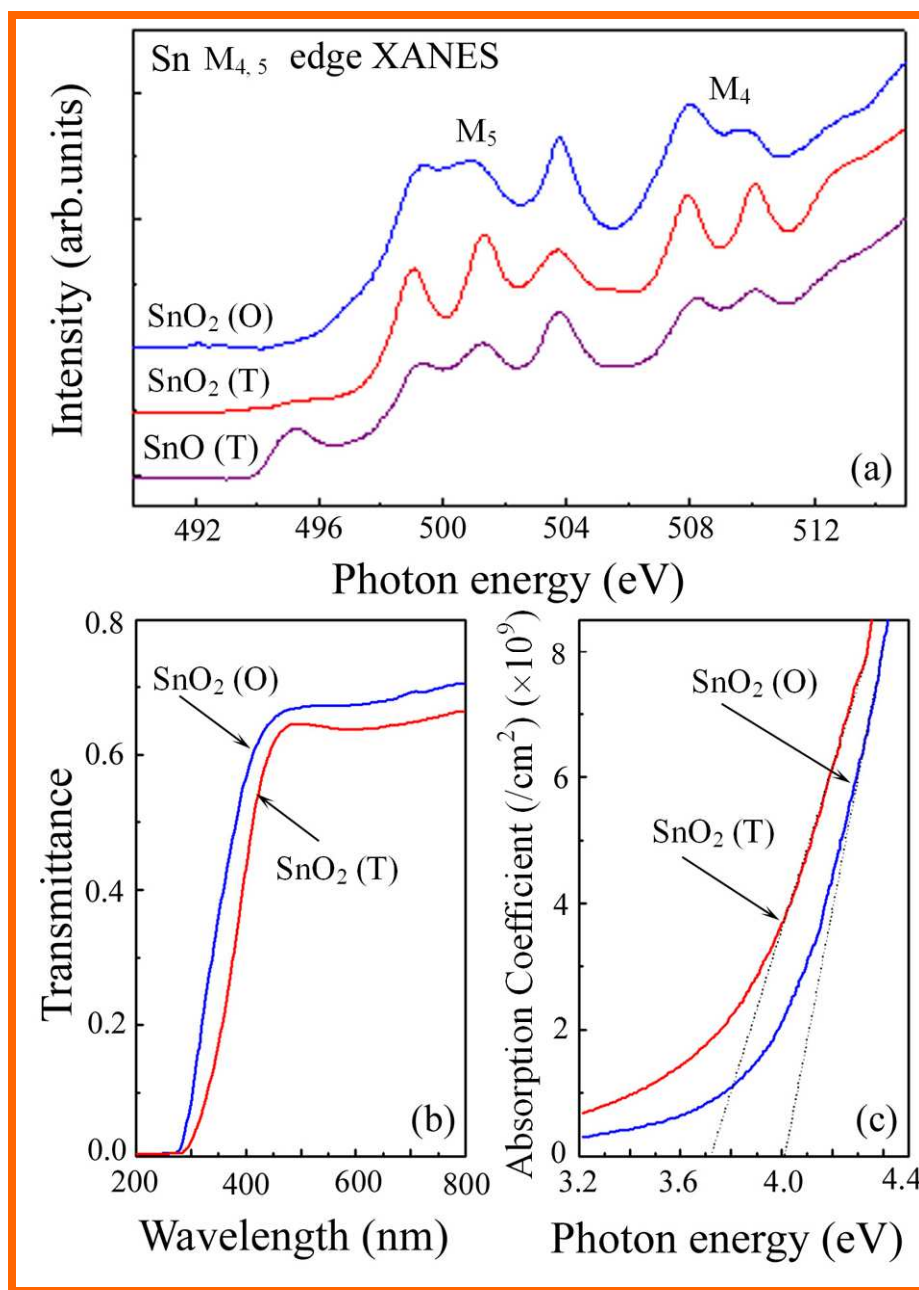
Fig. 8 (a) Sn $M_{4,5}$-edge XANES spectrum of the orthorhombic SnO_2 [labeled $SnO_2(O)$] compared with the spectra from tetragonal SnO_2 [labeled $SnO_2(T)$] and SnO [labeled SnO(T)]. (b) Spectrophotometric transmittance measured in a wavelength range of 200-800 nm for the orthorhombic SnO_2 and tetragonal SnO_2. (c) Absorption coefficient vs photon energy obtained from Fig. 8b.[55]

331   Further advancement of this approach to the synthesis of orthorhombic SnO_2 thin films requires a

332   clear understanding of its formation mechanism. Fig. 9 shows the schematic diagram of the oxygen

333   exchange reaction mechanism at the grain interfaces to explain the formation of this orthorhombic

334   phase. It consisted of four different oxygen species (O_2, O_2^-, O^-, and O) coupled by the elementary

335   reaction steps. Since the transported oxygen species is neutral atom, the availability of neutral oxygen

336   atom at the surface of the deposition layer is a factor influencing the degree of exchange. The amount

337   of available oxygen atom depends on the rate of the dissociation of O_2 and the amount of oxygen

338   species at the surface of the deposition layer in the atmosphere of the laser ablated plume. A based

339   explanation for the formation of orthorhombic-phase in the oxygen exchange reaction may come from

340   ablated plume to deposition layer variation. Since the grain-boundary diffusion is fast, we expect

341   oxygen exchange reaction at the grain interfaces in the deposition layer. The most significant

342   development of this model is the incorporation of the neutral oxygen atoms, which can be considered to

343   be a part of the lattice in the oxidized or stoichiometric form of the deposition layer, resulting in the

344   atomic rearrangement and the formation of the orthorhombic-phase SnO_2. In this model, the capture of

345   an election depends on the thermal velocity of electrons close to the substrate temperature and the

346   density of electrons close to the surface of the deposition layer. Since the oxygen species (O_2^- and O^-)

347   continuously exchange electrons with the deposition layer and the neutral oxygen atoms may contribute

348   to the lattice of the deposition layer via the faster diffusion of the grain boundary, which result in the

349   reduction of the oxygen vacancies, the band-gap widening occurs and the orthorhombic SnO_2 thin films

350   becomes transparent.[56] The epiaxial strain in randomly oriented polycrystalline orthorhombic SnO_2 thin

351   films should not attain substantial magnitude. We can speculate that the key factor for the synthesis of

352   the orthorhombic SnO_2 thin films is not compressive stress in the thin films. Above results indicated

353   that the orthorhombic SnO_2 thin films can be fabricated through processes at ambient or subambient

354   pressures.

355

356
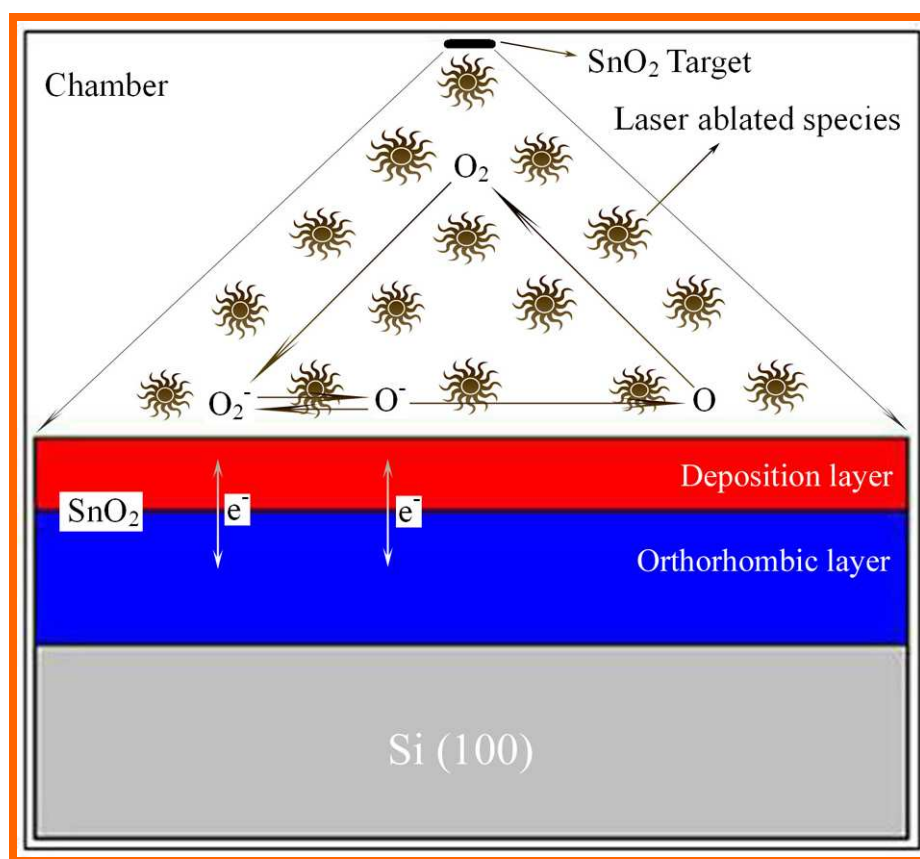
Fig. 9 Schematic diagram of oxygen exchange reaction mechanism at the grain interfaces to explain the

357

formation and optical properties of the orthorhombic phase.[55]

358

359   **5. Concluding Remarks**

360   Due to increasing interest in the SnO_2 nanomaterials, we carried out a series of studies investigating

361   their micro/nanostructural evolution and related formation mechanisms. We examined the

362   micro/nanostructures, functions, formation processes, and physicochemical characteristics of the SnO_2

363   thin films. Research on SnO_2 thin films will bring the innovations to technologies, such as

364   micro/nanostructure and morphology associated technique, micro/nanostructure and characterization

365   coupling technique, micro/nanostructure and advanced function simulation technique, and so forth. In

366   order to achieve optimized functional performance with the SnO_2 micro/nanostructures, however,

367   several challenges still remain. Further investigation and additional effort are needed to tackle some

368   important issues for promoting the practical applications of the SnO_2 micro/nanostructures.

369   This review has provided the synthetic strategies and formation mechanisms of the

370   micro/nanostructures of various SnO_2 thin films prepared by pulsed laser ablation. We hope this review

371   has given the reader a sense of the great potential of SnO_2 thin films with interesting

372   micro/nanostructures. As we and others continue to explore this promising material, the unique

373   micro/nanostructure features of SnO_2 thin films and numerous ways in which the properties can be

374   tuned will likely lead to the development of further exciting techniques and powerful combinations of

375   existing ones. It is expected that these SnO_2 thin films with fascinating micro/nanostructures may offer

376   vast and unforeseen opportunities in oxide semiconductor devices as well as in other fields of science

377   and technology.

378

379   **Acknowledgements**

390 **Biographical Information**

391

392 **Zhiwen Chen** was born in Hefei, Anhui, China, and received his BSc degree in Chemistry from the

393 Heifei Normal University, MSc degree in Inorganic Chemistry from the University of Science and

394 Technology of China (USTC), and PhD degree in Materials Physics and Chemistry from the City

395 University of Hong Kong (CityUHK). Since 1993, he has worked at USTC as an Assistant Professor,

396 Associate Professor. He joined the Teikyo University in Japan as a Research Fellow in 1999 and the

397 CityUHK as a Research Fellow and Senior Research Fellow in 2001 and 2007 respectively, and is now

398 a Chartered Professor at the Shanghai University, China. His research interests mainly focus on the

399 controllable-synthesis, characterization and properties of advanced functional materials and oxides

400 nanomaterials. He has published over 170 papers in refereed journals. He served as a Guest Editor, the

401 member of Editorial Board, and Reviewer or Referee for many international journals, and is now

402 Editor-in-Chief of *Advances in Materials Physics and Chemistry*, Website:

403 http://www.scirp.org/journal/ampc.

404

405   **Minghong Wu** earned her PhD from the Chinese Academy of Science in 1999. After some years of

406   postdoctoral research in Japan, she became a Professor in 2002 at the School of Environmental and

407   Chemical Engineering of Shanghai University in China. She was the Distinguished Young Scientist

408   supported by the National Natural Science Foundation of China. Her main research interests include

409   the environmental chemistry, nanostructures of sensors, and biomedical materials. So far she has

410   authored more than 130 publications and patents.

411

412   **Chan-Hung Shek** got his PhD in 1994 from the Department of Mechanical Engineering at the

413   University of Hong Kong. He then joined the City University of Hong Kong (CityUHK) as an

414   Assistant Professor and became an Associate Professor in 2001. He is currently a Professor in

415   CityUHK. Since 2007, he has been appointed as Assistant Head of Department of Physics and

416   Materials Science and now is an Associate Head, he was concurrently appointed as Assistant Dean of

417   College of Science and Engineering in 2011. He major research interests are the correlation among

418   processing, microstructures and properties of materials, including nanostructured metal oxides, bulk

419   metallic glasses and conventional engineering alloys.

420

421   **C. M. Lawrence Wu** received his PhD from the University of Bristol, UK in 1986 and has been

422   working in City University of Hong Kong since 1987. He is currently a Professor in the Department

423   of Physics and Materials Science. Apart from working on the synthesis and characterization of

424   nanocrystals, he also works on plasmonic effects in the application of bio-sensing and solar energy.

425

426   **Joseph K. L. Lai** won an open scholarship to study Physics at Keble College, Oxford University in

427   1971 and graduated with first class honours in 1974. He joined the Central Electricity Research

428   Laboratories (CERL) in UK after graduation and was appointed Project Leader of the Remaining Life

429   Study Group in 1984. While working at CERL he studied for a PhD at the City University, London,

430   UK and was awarded the degree in 1982. He returned to Hong Kong in 1985 and has worked at

431   CityUHK ever since. He is now Chair Professor of Materials Science in the Department of Physics and

432   Materials Science. Professor Lai is a Fellow of the Hong Kong Institution of Engineers, a Chartered

433   Engineer, and a Fellow of the following UK professional institutions: Institute of Materials, Minerals

434   and Mining, Institute of Physics, and Institution of Mechanical Engineers.

435 **References**

436 1 M. Batzill and U. Diebold, *Prog. Surf. Sci.*, 2005, **79**, 47-154.

437 2 Z. W. Chen, X. P. Wang, S. Tan, S. Y. Zhang, J. G. Hou and Z. Q. Wu, *Phys. Rev. B*, 2001, **63**,
438 165413.

439 3 M. P. Persson, A. Lherbier, Y. M. Niquet, F. Trizon and S. Roche, *Nano Lett.*, 2008, **8**, 4146-4150.

440 4 P. Nguyen, H. T. Ng and M. Meyyappan, *Adv. Mater.*, 2005, **17**, 1773-1777.

441 5 L. J. Wang, X. J. Chen, C. Chen, Y. Y. Liu, Z. W. Chen, C. H. Shek, C. M. L. Wu and J. K. L. Lai,
442 *J. Phys. Chem. C*, 2012, **116**, 21012-21017.

443 6 Z. W. Chen, D. Y. Pan, Z. Li, Z. Jiao, M. H. Wu, C. H. Shek, C. M. L. Wu, J. K. L. Lai, *Chem. Rev.*
444 2014, **114**, 7442-7486.

445 7 L. P. Qin, J. Q. Xu, X. W. Dong, Q. Y. Pan, Z. X. Cheng, Q. Xiang and F. Li, *Nanotechnology*,
446 2008, **19**, 185705.

447 8 C. Chen, L. J. Wang, Y. Y. Liu, Z. W. Chen, D. Y. Pan, Z. Li, Z. Jiao, P. F. Hu, C. H. Shek, C. M.
448 L. Wu, J. K. L. Lai and M. H. Wu, *Langmuir*, 2013, **29**, 4111-4118.

449 9 T. Tamal, N. Ichinose, S. Kawanishi, M. Nishii, T. Sasuga, I. Hashida and K. Mizuno, *Chem.*
450 *Mater.*, 1997, **9**, 2674-2675.

451 10 L. Mazeina, Y. N. Picard, J. D. Caldwell, E. R. Glaser and S. M. Prokes, *J. Cryst. Growth*, 2009,
452 **311**, 3158-3162.

453 11 X. H. Ding, D. W. Zeng and C. S. Xie, *Sens. Actuat. B*, 2010, **149**, 336-344.

454 12 X. Y. Xue, Z. H. Chen, C. H. Ma, L. L. Xing, Y. J. Chen, Y. G. Wang and T. H. Wang, *J. Phys.*

455   *Chem. C*, 2010, **114**, 3968-3972.

456 13 Y. Wang, J. Y. Lee and T. C. Deivaraj, *J. Phys. Chem. B*, 2004, **108**, 13589-13593.

457 14 K. Wijeratne, J. Akilavasan, M. Thelakkat and J. Bandara, *Electrochim. Acta*, 2012, **72**, 192-198.

458 15 J. Wang, Z. W. Chen, Y. Y. Liu, C. H. Shek, C. M. L. Wu and J. K. L. Lai, *Sol. Energy Mater. Sol.*

459   *Cells*, 2014, **128**, 254-259.

460 16 Z. W. Chen, Z. Jiao, M. H. Wu, C. H. Shek, C. M. L. Wu and J. K. L. Lai, *Prog. Mater. Sci.*, 2011,

461   **56**, 901-1029.

462 17 Z. W. Pan, Z. R. Dai and Z. L. Wang, *Science*, 2001, **291**, 1947-1749.

463 18 Z. R. Dai, J. L. Gole, J. D. Stout and Z. L. Wang, *J. Phys. Chem. B*, 2002, **106**, 1274-1279.

464 19 L. Giordano and G. Pacchioni, *Acc. Chem. Res.*, 2011, **44**, 1244-1252.

465 20 B. Cheng, J. M. Russell, W. S. Shi, L. Zhang and E. T. Samulski, *J. Am. Chem. Soc.*, 2004, **126**,

466   5972-5973.

467 21 N. Nilius, *Surf. Sci. Rep.*, 2009, **64**, 595-659.

468 22 H. T. Ng, J. Li, M. K. Smith, P. Nguyen, A. Cassell, J. Han and M. Meyyappan, *Science*, 2003, **300**,

469   1249.

470 23 Z. W. Chen, J. K. L. Lai and C. H. Shek, *Phys. Rev. B*, 2004, **70**, 165314.

471 24 Z. L. Wang, *Adv. Mater.*, 2003, **15**, 432-436.

472 25 C. H. Shek, J. K. L. Lai and G. M. Lin, *J. Phys. Chem. Solids*, 1999, **60**, 189-193.

473 26 S. Shukla, S. Seal, L. Ludwing and C. Parish, *Sens. Actuta. B*, 2004, **97**, 256-265.

474 27 J. Wang, J. Du, C. Chen, Z. Li, Z. Jiao, M. H. Wu, C. H. Shek, C. M. L. Wu, J. K. L. Lai and Z. W.

475   Chen, *J. Phys. Chem. C*, 2011, **115**, 20523-20528.

476 28 S. Harbeck, A. Szatvanyi, N. Barsan, U. Weimar and V. Hoffmann, *Thin Solid Films*, 2003, **436**,

477   76-83.

478 29 Z. W. Chen, J. K. L. Lai, C. H. Shek and H. D. Chen, *Appl. Phys. A: Mater. Sci. Proc.*, 2005, **81**,

479   959-962.

480 30 Z. W. Chen, J. K. L. Lai and C. H. Shek, *Phys. Lett. A*, 2005, **345**, 218-223.

481 31 O. Dos Santos, M. L. Weiller, D. Q. Junior and A. N. Medina, *Sens. Actuta. B*, 2001, **75**, 83-87.

482 32 V. Demarne and A. Grisel, *Sens. Actuat.*, 1988, **13**, 301-313.

483 33 Z. W. Chen, D. Y. Pan, B. Zhao, G. J. Ding, Z. Jiao, M. H. Wu, C. H. Shek, C. M. L. Wu and J. K.

484   L. Lai, *ACS Nano*, 2010, **4**, 1202-1208.

485 34 Z. W. Chen, Z. Jiao, D. Y. Pan, Z. Li, M. H. Wu, C. H. Shek, C. M. L.Wu and J. K. L. Lai, *Chem.*

486   *Rev.*, 2012, **112**, 3833-3855.

487 35 Z. W. Chen, Q. B. Li, D. Y. Pan, Z. Li, Z. Jiao, M. H. Wu, C. H. Shek, C. M. L. Wu and J. K. L.

488   Lai, *J. Phys. Chem. C*, 2011, **115**, 9871-9878.

489 36 Z. W. Chen, Q. B. Li, J. Wang, D. Y. Pan, Z. Jiao, M. H. Wu, C. H. Shek, C. M. L. Wu and J. K. L.

490   Lai, *Inorg. Chem.*, 2011, **50**, 6756-6761.

491 37 Z. W. Chen, Q. B. Li, D. Y. Pan, H. J. Zhang, Z. Jiao, M. H. Wu, C. H. Shek, C. M. L. Wu and J. K.

492   L. Lai, *Mater. Today*, 2011, **14**, 106-113.

493 38 S. Zhu, Y. F. Lu and M. H. Hong, *Appl. Phys. Lett.*, 2001, **79**, 1396-1398.

494   39 D. Kim and H. Lee, *J. Appl. Phys.*, 2001, **89**, 5703-5706.

495   40 R. L. Penn and J. F. Banfield, *Science*, 1998, **281**, 969-971.

496   41 Q. B. Li, C. Chen, Z. W. Chen, Z. Jiao, M. H. Wu, C. H. Shek, C. M. L. Wu and J. K. L. Lai, *Inorg.*
497   *Chem.*, 2012, **51**, 8473-8478.

498   42 E. R. Leite, T. R. Giraldi, F. M. Pontes, E. Longo, A. Beltrán and J. Andrés, *Appl. Phys. Lett.*,
499   2003, **83**, 1566.

500   43 Z. W. Chen, J. K. L. Lai and C. H. Shek, *Appl. Phys. Lett.*, 2006, **88**, 033115.

501   44 N. Combe and P. Jensen, *Phys. Rev. B*, 1998, **57**, 15553-15560.

502   45 L. Sangaletti, L. E. Depero, A. Dieguez, G. Marca, J. R. Morante, A. Romano-Rodriguez and G.
503   Sberveglieri, *Sens. Actuat. B*, 1997, **44**, 268-274.

504   46 K. Suito, N. Kawai and Y. Masuda, *Mater. Res. Bull.*, 1975, **10**, 677-680.

505   47 J. Haines and J. M. Léger, *Phys. Rev. B*, 1997, **55**, 11144-11154.

506   48 L. G. Liu, *Science*, 1978, **199**, 422-425.

507   49 V. E. Müller, *Acta Crystallogr. B*, 1984, **40**, 359-363.

508   50 C. H. Shek, J. K. L. Lai, G. M. Lin, Y. F. Zheng and W. H. Liu, *J. Phys. Chem. Solids*, 1997, **58**,
509   13-17.

510   51 V. Kraševec, A. Prodan, M. Hudomalj and S. Sulčič, *Phys. Status Solidi A*, 1985, **87**, 127-133.

511   52 L. Kaplan, A. Ben-Shalom, R. L. Boxman, S. Goldsmith, U. Rosenberg and M. Nathan, *Thin Solid*
512   *Films*, 1994, **253**, 1-8.

513   53 F. J. Lamelas and S. A. Reid, *Phys. Rev. B*, 1999, **60**, 9347-9352.

514   54 J. Arbiol, E. Comini, G. Faglia, G. Sberveglieri and J. R. Morante, *J. Cryst. Growth*, 2008, **310**,

515   253-260.

516   55 Z. W. Chen, J. K. L. Lai and C. H. Shek, *Appl. Phys. Lett.*, 2006, **89**, 231902.

517   56 B. Stjerna, E. Olsson and C. G. Granqvist, *J. Appl. Phys.*, 1994, **76**, 3797-3817.

518

519